

REMOTE RF POWERING AND DATA TELEMETRY SYSTEM FOR WIRELESS MEMS STRAIN SENSORS

Nattapon Chaimanonart, Wen H. Ko, and Darrin J. Young

Electrical Engineering and Computer Science Department, Case Western Reserve University
10900 Euclid Avenue, Cleveland, Ohio 44106, U.S.A.
E-mail: nxc35@case.edu

ABSTRACT

A reliable remote RF powering and data telemetry system is developed for high-performance industrial wireless MEMS strain sensing applications. The prototype system is insensitive to mechanical rotation and produces a stable DC voltage of 2.8 V with a 2 mA current supply capability from a 50 MHz RF power source with a power conversion efficiency of 11 %. An improved efficiency can be expected with an optimized power transmitter design. The telemetry system can transmit and receive digitized data at 100 kbps by using a load shift keying (LSK) communication scheme attractive for low power applications. The CMOS power converter electronics are fabricated in a 1.5 μm CMOS process occupying an area of approximately 1 mm X 1 mm. The achieved DC power is adequate for supplying a high-performance wireless MEMS strain sensing system.

KEYWORDS: Remote RF Powering, Telemetry, Wireless Sensing, MEMS Sensors

INTRODUCTION

High-performance wireless strain sensing microsystems consisting of miniature sensors and integrated interface electronics are highly critical for advanced industrial applications, such as point-stress and torque sensing for ball-bearings, rotating shafts and blades, etc. The sensed information is important for optimizing system performance, understanding material fatigue, and achieving a reliable system monitoring and intelligent control. Stringent performance requirements with a high sensitivity of 0.1 micro-strain ($\mu\epsilon$) over a signal bandwidth of a few kHz and a large dynamic range of 80 dB are typically demanded for these applications. Industrial strain sensing further imposes significant design challenges due to various rotating mechanical components employed in a system. Therefore, stand-alone wireless sensing microsystems with remote powering and data telemetry capabilities are highly desirable. Inductive-coupling-based powering techniques have been widely used for biomedical implants [1-4]. In these applications, the coupling coils are placed at certain fixed positions with a short distance on the order of a few millimeters. It is, therefore, necessary to develop remote powering techniques, which are insensitive to mechanical rotations and can achieve an increased coupling distance for advanced industrial sensing applications. It is also desirable to achieve wireless sensor data transmission through the same RF powering network. In this paper, an RF remote powering system, consisting of rotation-insensitive coupling coil loops and integrated CMOS power converter electronics, is presented to obtain a stable DC voltage of 2.8 V with a 2 mA current supply capability from a 50 MHz RF operation. The available DC power is adequate for supplying a high-performance strain sensing microsys-

tem [5]. The data telemetry is demonstrated with the coupling coils achieving a data rate of 100 kbps. An enhanced data rate is expected with a frequency shift keying or phase shift keying modulation techniques or at an expense of increased ripple on the converter DC output voltage with the current setup.

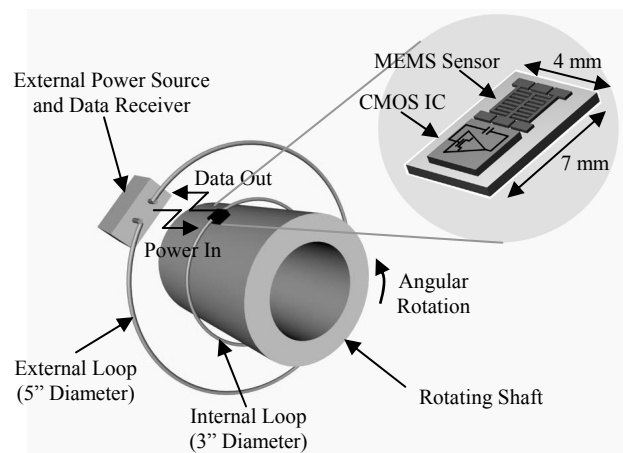


Figure 1. Wireless Microsystem Architecture

REMOTE RF POWERING ARCHITECTURE

Figure 1 presents the overall wireless microsystem architecture, which consists of an MEMS capacitive strain sensor and integrated CMOS interface electronics, coupled with two coil loops for remote RF powering and data telemetry. The microsystem occupies an area of approximately 4 mm x 7 mm including package and is attached to the surface of a rotating iron shaft with a diameter of 3 inches. An internal coil is wound around the shaft and

separated from the external coil by one inch for the prototype design. This coil configuration is critical for achieving a stable and uniform magnetic coil coupling during shaft rotation; hence a stable power conversion and reliable data telemetry for the proposed wireless microsystem. The rotation of the shaft produces a rotational torque, thus a surface strain which can be sensed by the MEMS strain sensor.

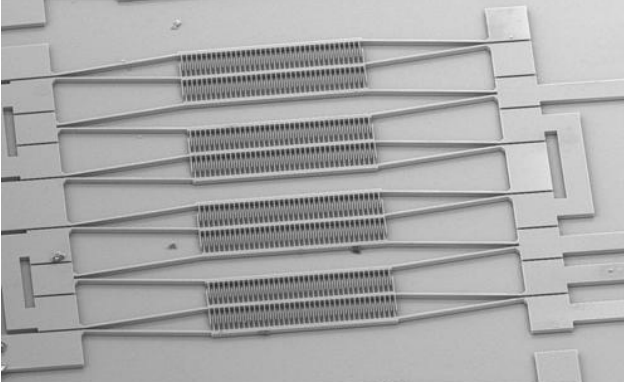


Figure 2. SEM Photo of a Fabricated Silicon MEMS Capacitive Strain Sensor

Figure 2 shows an SEM photo of a fabricated silicon MEMS capacitive strain sensor [6], which exhibits a gauge length of 1 mm and a nominal sensor capacitance value of 440 fF with a differential sensitivity of 265 aF per $\mu\epsilon$, employed for the prototype design.

The sensor output can be converted to a voltage, followed by digitization and data telemetry to a nearby receiver for signal acquisition and analysis. Figure 3 presents the proposed remote RF powering architecture, where an external RF power source is used to drive a tuned series resonator consisting of L_1 and C_1 . The resistor, R_1 , represents the overall series resistance associated with the resonator including the output resistance of the power source. The resonator is tuned to an optimal frequency as will be illustrated in the following. The RF signal is then coupled to a parallel resonator, consisting of L_2 and C_2 with a total loop resistance of R_2 , tuned to the same frequency. The signal is then rectified by an integrated CMOS fullwave rectifier to 5 V and further regulated to achieve a stable 3 V DC supply with a 2 mA current driving capability to power the overall microsystem as illustrated in Figure 1.

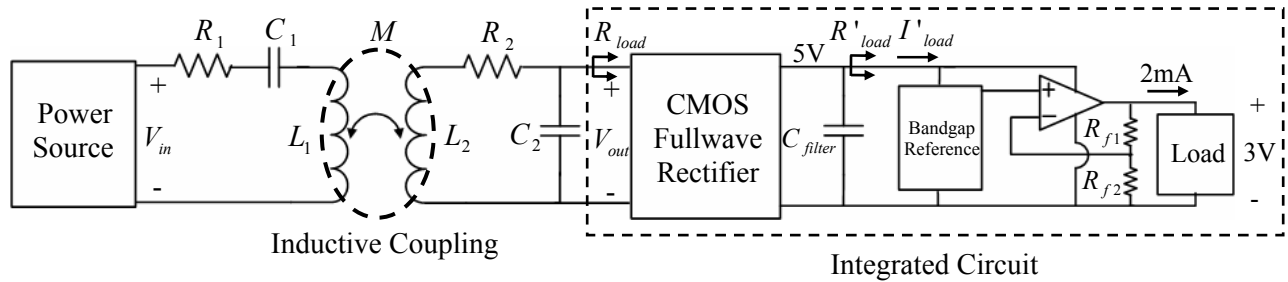


Figure 3. Remote RF Powering Architecture

In order to achieve an efficient power conversion system, the voltage gain across the tuned resonator network needs to be maximized. The gain can be expressed as

$$V_{out} / V_{in} = \frac{\omega^2 L_2 M}{(R_1 R_2 + (\omega M)^2 + R_1 (\omega L_2)^2 / R_{load})}, \quad (1)$$

where M represents the mutual inductance between the two coil inductors: L_1 and L_2 , ω is the operating frequency, and R_{load} is the equivalent AC resistive loading presented to the parallel resonator by the CMOS fullwave rectifier, which can be determined as [7]

$$R_{load} = R'_{load} / \sqrt{2}, \quad (2)$$

where R'_{load} is the resistive loading at the fullwave rectifier output and is approximately equal to 2 k Ω due to a 2.5 mA of loading current, I'_{load} , at the 5 V line. In the prototype design R_1 exhibits 12 Ω , which is dominated by the output resistance of the power source. All other parameters in Equation (1), L_1 , L_2 , M , and R_2 , are a function of coil geometry, such as number of coil turns, and operating frequency. These parameters have been extensively characterized to obtain an optimal condition for achieving a maximum voltage gain.

Figure 4 presents the measured voltage gain as a function of frequency and number of coil turns, which closely matches the predicted performance from Equation (1). It can be seen that a maximum voltage gain of 2.25 can be achieved at a 50 MHz operating frequency by employing a one-turn external coil loop, exhibiting an inductance value of 320 nH and AC resistance of 0.8 Ω , and a three-turn internal coil loop with an inductance value of 450 nH and AC resistance of 9.4 Ω . Both coil loops have self resonant frequencies well above 100 MHz and exhibit a mutual inductance of 25 nH. A design employing a four-turn internal coil loop suffers from a low voltage gain due to an excessive iron core loss at high frequencies. The one-turn external coil is chosen due to its simplicity. Furthermore, experiments have shown that a design employing a two-turn external coil can achieve a comparable gain. However, a much reduced operating frequency is required, limited by the self resonant frequency of the external coil. The reduced frequency will call for an excessively large on-chip filtering capacitor, C_{filter} , as will be illustrated in the next section, to achieve a desired output voltage ripple requirement, thus unsuitable for microsystem implementation.

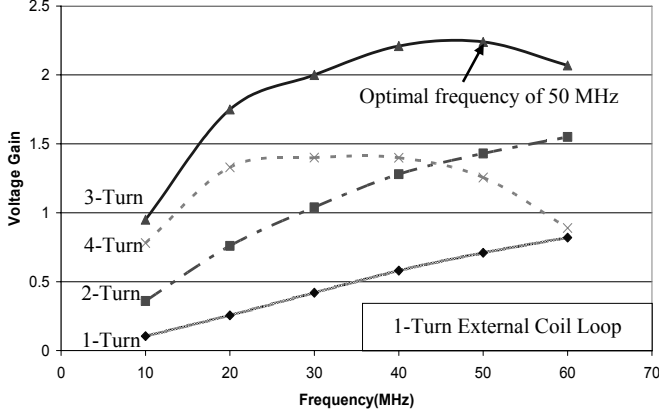


Figure 4. Measured Voltage Gain vs. Operating Frequency with Internal Coil Turn Numbers

INTEGRATED POWER CONVERTER ELECTRONICS

An integrated CMOS fullwave rectifier is used to rectify the received RF signal. Figure 5 presents the rectifier schematic, where $V_{AC-Input}$ represents the coupled RF signal across the parallel resonator, which is to be rectified to produce a DC output voltage, $V_{DC-Output}$.

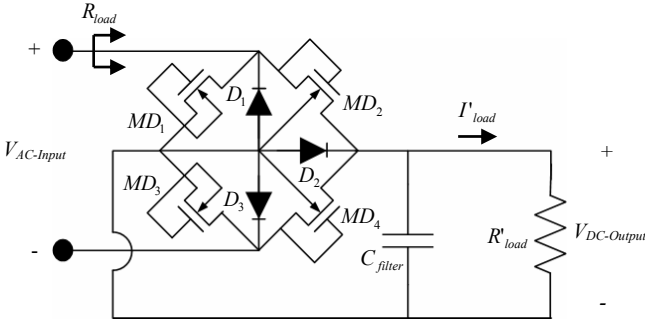


Figure 5. Simplified Inductive Coupling Circuit

The four MOSFETs connected in a diode configuration, MD_1 , MD_2 , MD_3 , and MD_4 , along with their parasitic source and drain to bulk junction diodes, D_1 , D_2 , and D_3 , form the fullwave rectifier. In a half cycle, MD_2 and D_3 perform the rectification with MD_4 and D_1 conducting during the other half cycle. The diode, D_2 , does not cause any performance degradation since it is always kept in a reverse bias condition. The total voltage drop across the rectifier is approximately 2.7 V, of which 2 V is consumed by the MOSFET diode due to an increased threshold voltage caused by body effect, and 0.7 V is dropped over the junction diode. Therefore, an RF signal with a 7.7 V amplitude is required to obtain a rectified DC output voltage of 5 V. A filtering capacitor, C_{filter} , needs to be properly selected in order to achieve a certain ripple requirement as shown in Equation (3)

$$C_{filter} = \frac{\pi \cdot I'_{load}}{V_r \omega}, \quad (3)$$

where V_r is the peak-peak ripple voltage amplitude, I'_{load} is the DC load current, and ω is the operating frequency. Thus, an increased operating frequency is desirable for achieving ripple requirements with a reduced filtering capacitor size. The prototype wireless microsystem design calls for a conservative peak-peak ripple voltage of 60 mV at the 5 V line, thus a 400 pF filtering capacitor occupying a chip area of 0.9 mm x 0.9 mm is required with I'_{load} of 2.5 mA.

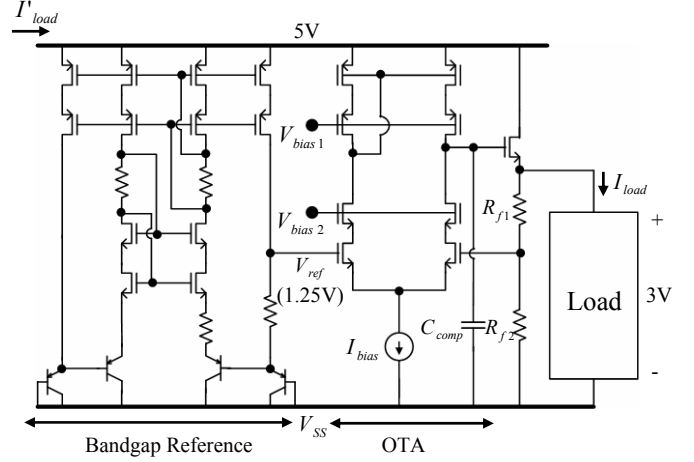


Figure 6. CMOS Linear Regulator

Figure 6 presents the schematic of a CMOS linear regulator used in the prototype system. The regulator holds the output voltage at a designed value of 3 V by comparing the output, through a resistive feedback network consisting of R_{f1} and R_{f2} , to a stable bandgap reference voltage, V_{ref} , of 1.25 V with a high-gain inverting amplifier. An OTA with a DC gain of 60 dB and unity gain frequency of 20 MHz is designed for achieving a proper regulation. Resistance values of 7 k Ω and 5 k Ω for R_{f1} and R_{f2} , respectively, are chosen to obtain a proper feedback ratio of 2.4. An output load resistance of 1.5 k Ω is used throughout the design process to ensure a 2 mA current driving capability.

DATA TELEMETRY

Low power data telemetry can be achieved by using the same set of coil loops. Figure 7 shows the simplified RF powering architecture with the wireless data modulation and demodulation circuits. A digital data waveform, representing the sensor information, is used to drive an NMOS switching transistor for varying the equivalent DC load from R'_{load} when the switch is opened, to R'_{load} in parallel with R_{switch} when the switch is closed. This results in an overall secondary loading change, which can be modeled as a reflected resistance,

$$R_{reflect} = \frac{(\omega M)^2}{(R_2 + (\omega L_2)^2 / R_{load})}, \quad (4)$$

in the primary circuit. In this configuration, when both primary and secondary circuits are tuned to the same fre-

quency and V_{in} is maintained at a constant amplitude, the voltage across L_1 is modulated by the variation of $R_{reflect}$. It is obvious that an increased modulation index can be obtained by lowering R_{switch} . However, it is limited by the rectifier output voltage handling capability, which has to be high enough to ensure a regulated output voltage of 3V. Furthermore, an increased RF power is required from the power source to supply the additional resistive loading. In this design, $R_{reflect}$ of 15 k Ω is chosen to maintain the 3V output DC voltage with the rectified output voltage varying from 5V to 5.9V.

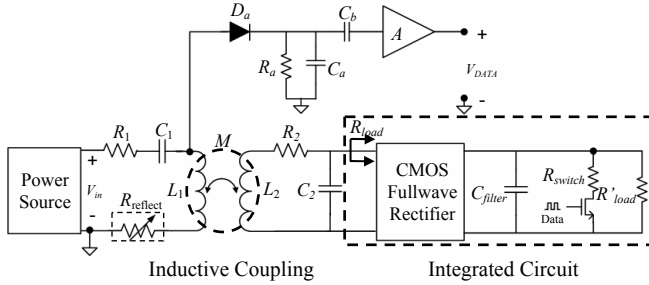


Figure 7. Simplified RF Powering and Data Telemetry Architecture

With a peak detection circuit consisting of a diode, D_a , a low pass filter of R_a and C_a , and a voltage amplifier, the digital data waveform can be retrieved at V_{DATA} . The RC low pass filter is required to pass the low frequency digital signal and reject the 50 MHz carrier, thus C_a of 5 pF and R_a of 10 k Ω are chosen to achieve a corner frequency of 3.2 MHz. It is noted that R_a is properly selected so that it does not introduce a significant loading to the primary circuit, which can cause a degradation of power conversion efficiency. Computer simulation shows that the digitized data with an amplitude of 9V can be obtained after low pass filtering and further amplification by a voltage amplifier with a gain of 90. For the prototype design, the maximum signal bandwidth, f_D , can be determined by Equation (5)

$$f_D = \frac{f}{2Q}, \quad (5)$$

where f is the carrier frequency and Q is the quality factor of the primary tank (the tank with a higher Q in the current design). Given the quality factor of approximately 8 at 50 MHz, a maximum signal bandwidth of 3 MHz is thus expected. In practice, the signal bandwidth is not only limited by the Q factor but also by time constant of the internal circuits since LSK modulation scheme relies on an amplitude change for data modulation. In this design, C_{filter} of 400 pF and R'_{load} of 2 k Ω at 5V line result in a time constant of 0.8 μ sec, which would determine f_D of approximately 125 KHz corresponding to a signal settling time of five time constants, thus a data rate of 250 kbps. As indicated above, with a design constraint of a fixed driving load of 2 k Ω , the data rate can be improved with a reduced C_{filter} until it is limited by the quality factor of primary tank.

Although an increased data rate can be achieved with a reduction of C_{filter} , the voltage ripple at 5V line increases proportionally as denoted by Equation (3). This phenomenon will affect the performance of the MEMS interface electronics, thus an adequate C_{filter} value for the overall system design and electronic circuitry with a sufficient power supply rejection ratio will be required.

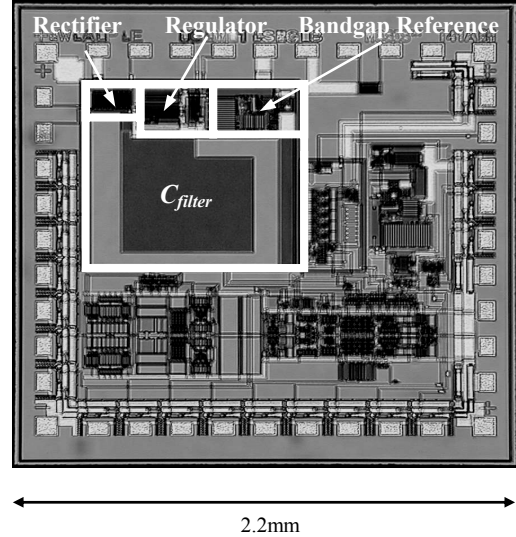


Figure 8. Chip Micrograph

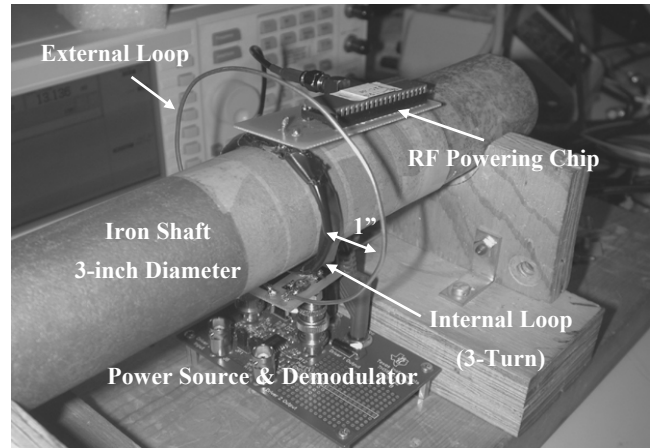


Figure 9. Test Setup

MEASUREMENT RESULTS

The integrated CMOS power converter electronics are fabricated in a 1.5 μ m CMOS process. Figure 8 presents the chip photo, where the converter occupies an area of approximately 1 mm x 1 mm and is also integrated with the low noise MEMS strain sensor detection electronics. The test setup for the prototype remote RF powering system is shown in Figure 9. A 50 MHz RF power source with an amplitude of 8 V peak to peak is used to drive the tuned LC network. The CMOS chip is packaged in a through-hole DIP40 package mounted on the surface of an iron shaft for

evaluation. The system provides a stable DC voltage of 2.8 V with a 2 mA current supply capability independent of the iron shaft rotation, thus achieving a power conversion efficiency of 11 %. An improved efficiency can be expected with an optimized power transmitter design [8].

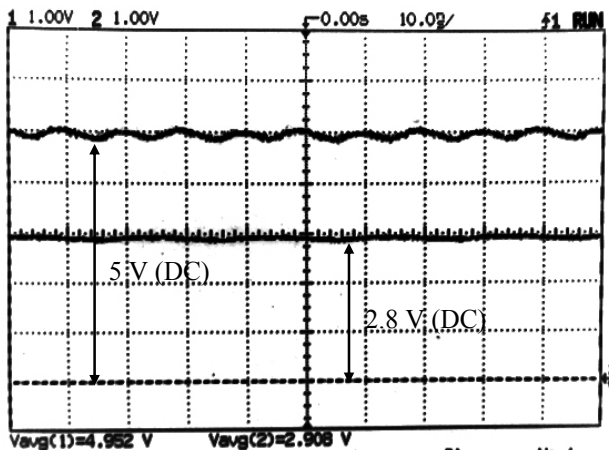


Figure 10. 5 V and 2.8 V DC Outputs

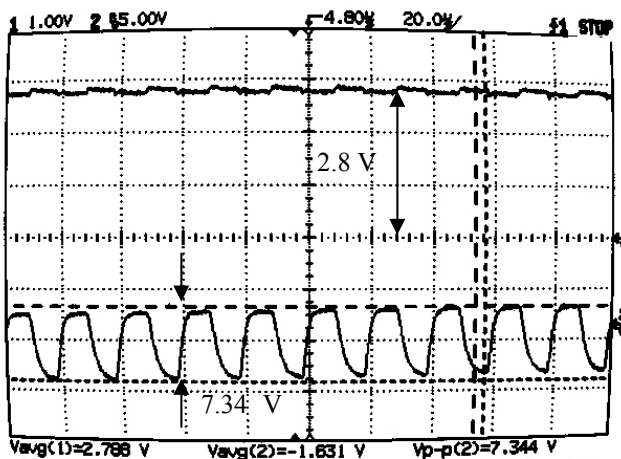


Figure 11. 2.8 V DC Output and Demodulated Clock Signal at 50 kHz

The regulator output exhibits a line regulation and load regulation of 16 mV/V and 8 mV/mA, respectively and a ripple with an amplitude of 80 mV peak to peak. The large ripple is caused by a strong package coupling at 50 MHz, which can be substantially minimized by using an improved package. Figure 10 shows the voltage waveforms at the 5 V line and 2.8 V output. The output voltage deviates from the designed value of 3 V due to the modeling limitation of the junction diodes used in the bandgap reference design. After completing the electrical characterization, the remote RF powering system is used to power the MEMS strain sensor and integrated low noise interface electronics to achieve a superior performance: a minimum detectable strain of 0.09 $\mu\epsilon$ over a 10 kHz bandwidth with a dynamic range 81 dB. This is the same performance achieved by

using a 3 V power supply [5]. Figure 11 shows the demodulated data waveform and 2.8 V output. A 50 % duty cycle digital clock of 50 kHz is successfully reconstructed with a peak to peak amplitude of 7.3 V while maintaining the output voltage at 2.8 V with a ripple of 100 mV peak to peak at the clock frequency. The settling time is approximately 5 μsec , which is close to expected value of 4 μsec .

Computer simulations reveal that switching the capacitance, C_2 , shown in Figure 7 between 19 pF and 23 pF would result in a phase change of the voltage across inductor, L_1 , while maintaining a nearly constant voltage gain of the remote RF powering system. Figure 12 shows a simulated 50% duty cycle digital clock at 1.25MHz, equivalent to a data rate of 2.5 Mbps, by employing a simple phase demodulator circuit for data recovery.

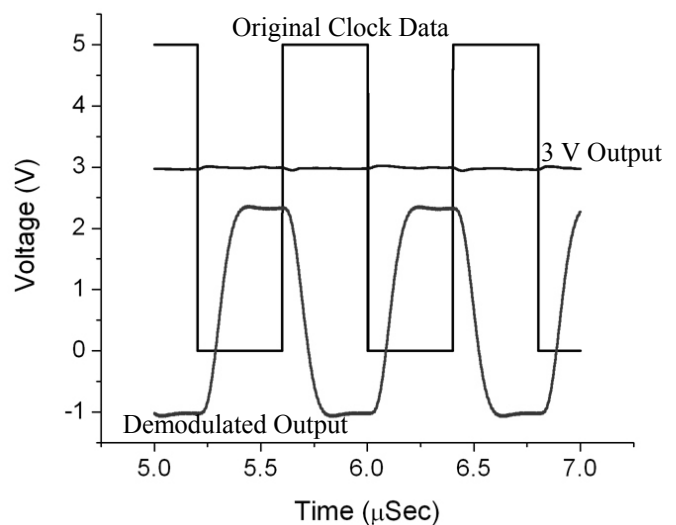


Figure 12. Simulated 3 V Output and Demodulated Clock Signal at 1.25 MHz from Phase Shift Keying

CONCLUSIONS

A reliable remote RF powering and data telemetry system for advanced industrial wireless MEMS strain sensing application is presented. The prototype system is designed to be insensitive to mechanical rotations and outputs a stable DC voltage of 2.8 V with a 2 mA current supply capability from a 50 MHz RF operation. The power converter electronics are integrated with the low noise strain sensor interface circuitry and can provide a sufficient power to the wireless strain sensing microsystem to demonstrate a superior performance. The telemetry system can transmit and receive digital data at 100 kbps by using a load shift keying communication scheme. An enhance data rate is expected with a frequency or phase modulation.

ACKNOWLEDGMENTS

This work is supported by U.S. Army Research Office under contract # DADD19-02-1-0198 and National Science Foundation under grant # EIA-0329811.

REFERENCES

- [1] J. A. Von Arx and K. Najafi, "A wireless single-chip telemetry-powered neural stimulation system," *Technical Digest, IEEE International Solid-State Circuits Conference*, pp. 214 – 215, February 1999.
- [2] W. Liu and M. S. Humayun, "Retinal Prosthesis," *Technical Digest, IEEE International Solid-State Circuits Conference*, pp. 218 – 225, February 2004.
- [3] J. Ji and K. D. Wise, "An implantable CMOS circuit interface for multiplexed microelectrode recording arrays," *IEEE Journal of Solid-State Circuits*, Vol. 27, Issue 3, pp. 433 – 443, March 1992.
- [4] B. Smith, Z. Tang, M. W. Johnson, S. Pourmehdi, M. M. Gazdik, J. R. Buckett, and P. H. Peckham, "An externally powered, multichannel, implantable stimulator-telemeter for control of paralyzed muscle," *IEEE Transactions on Biomedical Engineering*, Vol. 45, Issue 4, pp. 463 – 475, April 1998.
- [5] M. Suster, N. Chaimanonart, J. Guo, W. H. Ko, and D. J. Young, "Remote-powered high-performance strain sensing microsystem," *IEEE International Conference on Micro Electro Mechanical Systems*, pp. 255-258, January 2005.
- [6] J. Guo, H. I. Kuo, D. J. Young, and W. H. Ko, "Buckled beam linear output capacitive strain sensor," *Solid-State Sensor, Actuator and Microsystems Workshop*, pp. 344-347, June 2004.
- [7] Z. Tang, B. Smith, J. H. Schild, and P. H. Peckham, "Data transmission from an implantable biotelemetry by load-shift keying using circuit configuration modulator," *IEEE Transactions on Biomedical Engineering*, Vol. 42, No. 5, pp. 524 – 528, May 1995.
- [8] P. R. Troyk and G. A. DeMichele, "Inductively-coupled power and data link for neural prostheses using a class-E oscillator and FSK modulation," *IEEE International Conference Engineering in Medicine and Biology Society*, Vol. 4, pp. 3376 – 3379, September 2003.